Article

Initiation of Vaterite#Aragonite CaCO Particles from Silicate#Casein Sols

Alina E. Voinescu, Didier Touraud, Alois Lecker, Arno Pfitzner, Lorenz Kienle, and Werner Kunz

More About This Article

Additional resources and features associated with this article are available within the HTML version:

- Supporting Information
- Access to high resolution figures
- Links to articles and content related to this article
- Copyright permission to reproduce figures and/or text from this article

View the Full Text HTML

Initiation of Vaterite−Aragonite CaCO₃ Particles from Silicate−Casein Sols

Alina E. Voinescu,[†] Didier Touraud,[†] Alois Lecker,[‡] Arno Pfitzner,[‡] Lorenz Kienle,[§] and Werner Kunz*,[†]

Institute of Physical and Theoretical Chemistry, University of Regensburg, Germany, Institute of Inorganic Chemistry, University of Regensburg, Germany, and Max Planck Institute for Solid State Research, Stuttgart, Germany

^{31}P NMR difference spectra of sodium caseinate sols with and without silicate ions provide direct evidence of interactions between silicate ions and casein serine phosphate groups. The addition of Ca^{2+} to sodium caseinate solution without silicate ions and, subsequently, the diffusion of atmospheric CO_2 to the resulting mixture do not lead to $CaCO_3$ mineralization, whereas comparable experiments in the presence of silicate ions induce the precipitation of hemispherical three-component microstructures composed of silica, casein, and calcium carbonate. Apparently, the silicate−protein interaction plays a role as promoter for calcium carbonate mineralization in aqueous sols. X-ray diffraction (XRD) and Fourier-transform infrared (FTIR) analyses reveal that vaterite is the crystalline phase of the composites. The observed materials are flat on one side and curved outward on the other side. In time, the flat surface cracks to display a star-like shape. Occasionally, in the center of the crack, layer-by-layer sphere-like particles grow, probably due to a secondary nucleation. These spheres are composed of a large number of two-dimensional aragonitic sheets, which are densely packed and form a multilayered structure.

1. Introduction

Biominerals are usually a complex assemblage consisting of inorganic ions intimately associated with organic macromolecules. Among all essential elements required by living organisms, calcium and silicon are of particular interest. They are the common constituents of the crust of the earth,[1] tissues (bones, teeth, and shells),[2] and leaves[3] along with acidic proteins. Above all, these two ions are presented also in a number of body fluids[4] (e.g., saliva), where the phosphopeptides tend either to bind calcium or to form serine−silicate complexes. These complexes likely involve H-bonds or direct C−O−Si covalent bonds, where Si is in tetra- and pentacoordination,[5−11] respectively.

Important sources of phosphoproteins are the casein proteins (used in the present work) that are released by enzymatic hydrolysis, gastrointestinal digestion, or food processing.[12] The caseins ($α_{s1}$-, $α_{s2}$-, $β$- and $κ$-) represent more than 80% of the proteins in milk[13] and in a colloidal state exhibit a strong tendency to assemble into casein micelles,[14] which are roughly spherical colloidal complexes of proteins and salts with diameters ranging from 90 to 150 nm.[15] The casein micelle has a hydrophobic interior surrounded by a hydrophilic charged layer. According to Holt et al.,[16] the hydrophilic layer is composed of $κ$-caseins, which ensure the stability of the casein micelle through a steric stabilization mechanism against further aggregation. Earlier studies show that the hydrophobic interior of casein micelles consists of spherical subunits called submicelles (15−20 nm in diameter),[17−19] which are kept together by hydrophobic interaction between proteins and by calcium phosphate linkages.[20] Calcium ions are essential for casein micelle formation and represent 2.81 wt % of the casein micelle content. One of the biological roles of casein is to inhibit crystal growth in the secretory cell.

As mentioned before, the phosphoproteins build complexes with silicate ions. Previously, it has been suggested that such complexes play a key role in biomineralization reactions.[2−5,21] For example, silica-associated phosphopropteins have been identified and implicated in diatomic biosilica formation.[22] Today, the silicic−macromolecule interaction is explored in relation with calcium carbonate precipitation too. Recently, Jiang et al.[23,24] prepared poly(methacrylic acid) (PMMA)/SiO₂/CaCO₃ composite particles via emulsion polymerization and observed that the surfaces of the modified inorganic particles are grafted with PMMA molecules. The present paper reports on another particular example, in which the synthetic polymer is replaced by the casein phosphoprotein. This protein, known as a calcium sponge molecule with integrated nucleation sites, will remove the calcium ions from the bulk and, thus, it will have a big influence in the mineralization process.

As a source of silicate ions, we used tetraethylorthosilicate (TEOS), which, when hydrolyzed under basic conditions, results in the formation of negatively charged silica species.[25,26]

2. Experimental Procedures

2.1. Materials Preparation. Casein technical grade was supplied by Lancaster and used without further purification. We used mixtures rather than one of its pure components due to synergistic effects of the casein fractions in micelle formation and ion binding. Tetraethylorthosilicate (TEOS, purity >98%), calcium chloride dihydrate ($CaCl_2$·$2H_2O$, purity >99%), and sodium hydroxide (NaOH, purity 99%) were purchased from Sigma-Aldrich and used as received. Deuterium oxide (D_2O, 99.8 atom % D), urea (CH_4N_2O), and ethanol (EtOH, purity 99.9%) were supplied by Deutero GmbH, Merk, and J. T. Baker, respectively. Purified water with an electrical conductivity of less than 10^{-6} S·m^{-1} was taken from a Milli-Q system.

　* To whom correspondence should be addressed. Fax: (+) 49 941 943 4532. E-mail: Werner.Kunz@chemie.uni-regensburg.de.
　† Institute of Physical and Theoretical Chemistry, University of Regensburg.
　‡ Institute of Inorganic Chemistry, University of Regensburg.
　§ Max Planck Institute for Solid State Research.

17500 *J. Phys. Chem. C, Vol. 112, No. 45, 2008*

Voinescu et al.

2.1.1. Preparation of the Alkaline Silica Solution (Solution 1). Alkaline silica solution was prepared by mixing 0.17 mL of TEOS, 0.17 mL of ethanol, 7.5 mL of NaOH (0.1 M), ~92 mL of water and stirring for 60 min at room temperature. During this time, the solubility and, subsequently, the polymerization of silica alkoxide into colloidal silica particles take place. Afterwards, the pH was adjusted to 11 ± 0.1 with aqueous sodium hydroxide (1 M).

2.1.2. Preparation of the Na Caseinate Solution (Solution 2). According to HPLC-UV analyses performed at the institute Agrobio (France), 100 g of product contains 27.34 g of α_{s1}-, 3.86 g of α_{s2}-, 23.61 g of β- and 28.56 g of κ-casein. Other series of proteins, namely, α-lactalbumin, β-lactoglobulin, bovine serum albumin, lactoperoxydase, and immunoglobulin G, were present below the limit of detection of 10 ppm. The casein granules (0.1–5 g/L) were dissolved by addition of aqueous NaOH to yield a solution of pH 11 and stirred for 1 h until an isotropic solution was obtained. According to DLS measurements, a 1 g/L solution contained casein submicelles (dominant species, ~90% submicelles) and casein micelles with hydrodynamic radii of ~18 and ~200 nm, respectively.

2.1.3. Preparation of the Alkaline Silica−Casein Solution (Solution 3). Alkaline silica-casein solution was prepared in a 100 mL plastic beaker by mixing 0.17 mL TEOS, 0.17 mL ethanol, 7.5 mL NaOH (0.1 M), 0–5 g/L casein, water and stirring for 90 min until the solution became isotropic. The pH was adjusted to 11 ± 0.1 with aqueous sodium hydroxide (1 M).

2.1.4. Mineralization of $CaCO_3$. The reaction was started by adding 1.4 mL of a calcium chloride solution (0.5 M) to the aforementioned solutions (1−3). The total amount of the mixture was 100 mL. After the addition of calcium salt, the solutions were then transferred to open cells (plastic circular wells (Linbro Tissue Culture), 1.7 cm deep and 1.6 cm in diameter) and left at 20 °C for about 24 h. During this time, precipitation and growth of crystals occurred due to the slow diffusion of atmospheric CO_2 into the mixture. The products were then washed several times in water and ethanol and examined by the analytical techniques described in the following sections.

2.2. Analytical Methods. The **pH** of the solutions was measured before and after the addition of calcium chloride using an Ag/AgCl plastic-body electrode (TPS, Model smartCHEM-Lab).

2.2.1. Protein Structure. Phosphor nuclear magnetic resonance (^{31}P NMR) spectra measurements were carried out with a Bruker Avance 400 spectrometer working at 161.98 MHz under proton-decoupling conditions. The number of scans was 1000 in all measurements, and the applied exponential line broadening was 2Hz. Chemical shifts were referenced to external 85% aqueous H_3PO_4. The samples consisted of 50 mg of casein dissolved in 10 mL of D_2O solution (10%, w/v) with or without 17 μL of TEOS. Additionally, we performed an experiment in the presence of urea (6 M), a hydrogen bond disrupter, to probe the hydrogen bond formation between silicate ions and the protein. The pH of the solution was adjusted to 11. About 1 mL of sample in 203 mm length high-resolution NMR tubes (Norell, Inc) were used for NMR measurements.

2.2.2. Particle Size. Dynamic light scattering (DLS) measurements were made using a Zetasizer spectrometer (Malvern Instruments Ltd., model Z3000) equipped with a 5 mW He−Ne laser. Measurements were carried out at a scattering angle of 90°, and the intensity autocorrelation functions were analyzed using the NNLS software.
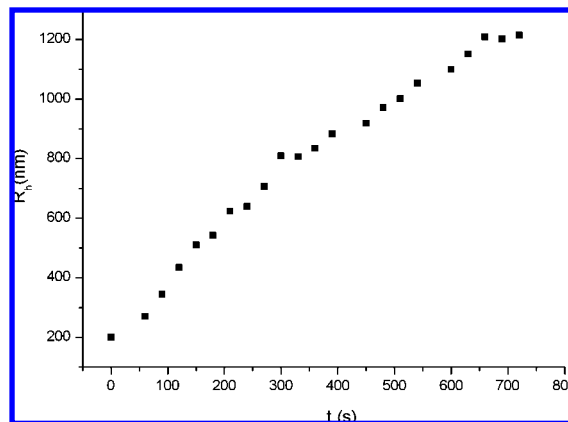

Figure 1. The light scattering curve obtained after the addition of calcium chloride to alkaline silica solution. [TEOS] = 7.5 mM; [Ca^{2+}] = 7 mM; pH = 11.

2.2.3. Turbidity. UV-VIS absorption spectra were recorded on a Perkin Elmer Lambda 18 spectrophotometer and used for detecting the sample turbidity by measuring the absorbance at 280 nm.

2.2.4. Crystal Habit. Microscopy was used to determine the crystal habit. Light microscopy was performed using a Nikon transmission microscope (model Eclipse E400). Images were taken between cross polarizers and produced with the help of a JVC CCD color video camera (Model TKC1380). Scanning electron microscopy (SEM) was performed using a microscope Jeol JSM 840 operating at 0.2−30 kV. The sample was coated with Au in a Polaron Equipment LTD sputter coater.

2.2.5. Crystal Polymorphism. Fourier transform infrared spectroscopy (FTIR) was recorded on a Jasco FTIR-610 spectrometer. The spectrum was recorded in reflection mode from 4000 to 400 cm^{-1} at a resolution of 2 cm^{-1}. X-ray diffraction (XRD) measurements were done using a STOE STADI P diffractometer (STOE&CIE) providing Cu Kα_1 radiation monochromated with a germanium single crystal (λ = 1.540 598 Å). Typical diffraction patterns were recorded in the range of 8° < 2θ < 90° at a scanning speed of 0.8°/min. Transmission electron microscopy (TEM) was performed with a Philips CM30 ST electron microscope (300 kV, LaB$_6$ cathode, Gatan multiscan CCD camera).

2.2.6. Chemical Composition. Energy-dispersive X-ray (EDX) analysis was performed using an EDAX microanalyzer mounted on a FEI Quanta 400T scanning electron microscope at 15 kV. This technique was used in order to quantify the approximate composition of the self-assembled silica−casein−calcium carbonate crystals.

3. Results

3.1. The Addition of Ca^{2+} to the Alkaline Silica Solution and, Subsequently, the Diffusion of Atmospheric CO_2. In the absence of metal cations, DLS indicates a hydrodynamic radius (R_H) of circa 15 ± 10 nm and a polydispersity index around 0.2−0.4, which remain constant over time. According to Patapov,[15] the surface of the colloidal silica particles has a negative electric charge that prevents aggregation of the particles due to electrostatic repulsive forces and ensures the stability of colloidal silica in the solution.

3.1.1. Early Stage of the Precipitation Process. The addition of calcium chloride to a hydrolyzed TEOS solution induced cloudiness in the mixture immediately. The growth of particles was monitored by dynamic light scattering (DLS) and is shown in Figure 1. The onset of nucleation (R_H = 200 nm; because

Initiation of Vaterite−Aragonite CaCO₃ Particles

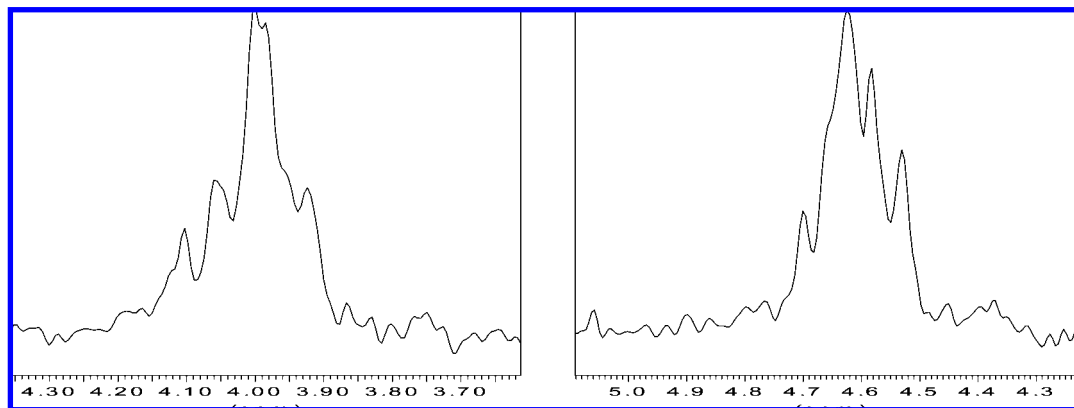*J. Phys. Chem. C, Vol. 112, No. 45, 2008* **17501**

Figure 2. The liquid-state ^{31}P NMR spectra (161.9 MHz) of Na caseinate sols in the absence (left) and in the presence (right) of silicate ions at pH 11 and 25 °C. Protein and silica concentrations were 5 g/L and 7.5 mM, respectively.

the aggregation of silica particles induced by the cation is fast, this was the first data point acquired by DLS) was followed by a fast growth of the aggregates with time between a linear increase and a typical saturation curve. Maybe the bigger particles sedimented and were therefore lost from solution detection. After a few minutes, macroscopic flocs, which settled down very quickly, were formed. Previously, it was reported that in the presence of calcium cations, silica species nucleate and grow.[27,28] To study these flocs in detail, they were collected and analyzed by means of SEM, XRD, FTIR, and EDX analysis (Figures S_1−S_3, Supporting Information). From these analyses, it results that the cloudiness in the mixture is due to the formation of amorphous SiO_2 particles.

3.1.2. Later Stage of the Precipitation Process. After 24 hours in contact with atmospheric CO_2, distinct $SiO_2/CaCO_3$ composite crystal morphologies precipitated. The optical image (Figure S_4, Supporting Information) shows modified calcite (in agreement with Imai et al.[29]) and aragonite crystals with diameters around 70−90 μm. The corresponding XRD pattern (Figure S_5, Supporting Information) exhibits characteristic reflections of calcite (C_{104}, the dominant phase) and aragonite (A_{221}), but no peaks characteristic for vaterite.

3.2. ^{31}P NMR Difference Spectra of Na Caseinate Sols with and without Silicate Ions. Figure 2 shows the ^{31}P NMR spectra of Na caseinate sols in the absence (left) and in the presence of silicate ions (right). In the absence of silicate ions, the spectrum shows an NMR signal between 3.9 and 4.1 ppm consisting of a broad quartet peak. The chemical shift range of the peak fits with the chemical shift range of 3−4.6 ppm, which has been published previously for serine monophosphate peaks (Ser−O−PO₃²⁻) in casein solutions.[30−33] In the presence of silicate ions, the NMR spectrum shows also a broad-based quartet peak. Upon comparison of both spectra, it follows that in the presence of silicate ions, the NMR signal of Ser−O−PO₃²⁻ was shifted ca. 0.7 ppm upfield. Further, the quartet peak profile looks different from the signal obtained in the absence of silicate ions. All four peaks that compose the broad NMR signal became narrower. From all these changes, it follows that the silicate ions interact with the protein and lead to a change in the protein structure conformation. Unfortunately, comparing the hydrodynamic radii for solutions of casein in the absence and in the presence of silica, we observed no difference between the radii. This is likely due to the casein polydispersity system. As we mentioned before, the casein solution is composed of submicelles (∼18 nm) and micelles (∼200 nm).

3.3. The Addition of Ca²⁺ to the Na Caseinate Solution and, Subsequently, the Diffusion of Atmospheric CO₂.
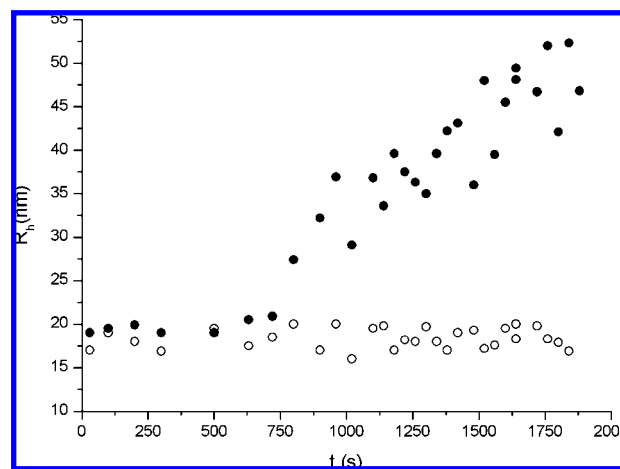

Figure 3. Dynamic light scattering curves obtained after rapidly mixing solutions of CaCl₂ with either Na caseinate (○) or silica−casein (●) solution.

3.3.1. Early Stage of the Precipitation Process. The addition of calcium ions to the Na caseinate solution induces no change in the hydrodynamic radius (Figure 3) and in the absorbance A_{280} within 30 min (Figure 4A, inset). After 1 h, the initially colorless solution becomes slightly bluish (Figure 4B), and this behavior is confirmed also by the increase of its absorbance with time (Figure 4A).

3.3.2. Later Stage of the Precipitation Process. After 24 hours, the solution becomes milky (Figure 4B) and gels and the absorbance dramatically increases (Figure 4A). It is likely that the turbidity change is due to the casein micelle formation, which becomes the dominant species. Furthermore, in contact with atmospheric CO_2, no visible $CaCO_3$ crystals are precipitated. Even after 4 days, when half of the water is evaporated and the sample is contaminated by bacteria, calcium carbonate precipitation does not take place. However, we did not exclude the formation of colloidal amorphous calcium carbonate. For this reason, we performed an additional experiment, in which the aged solution is analyzed by means of FTIR. As a result, we observed no absorption bands characteristic of amorphous calcium carbonate (ACC).

3.4. The Addition of Ca²⁺ to the Alkaline Silica−Casein Solution and, Subsequently, the Diffusion of Atmospheric CO₂. *3.4.1. Early Stage of the Precipitation Process.* The addition of calcium ions to the colorless alkaline silica−casein solution induces a bluish color in the mixture immediately. This observation is in agreement with the dramatic increase of the absorbance at 280 nm with time (Figure 4A, inset). Moreover,
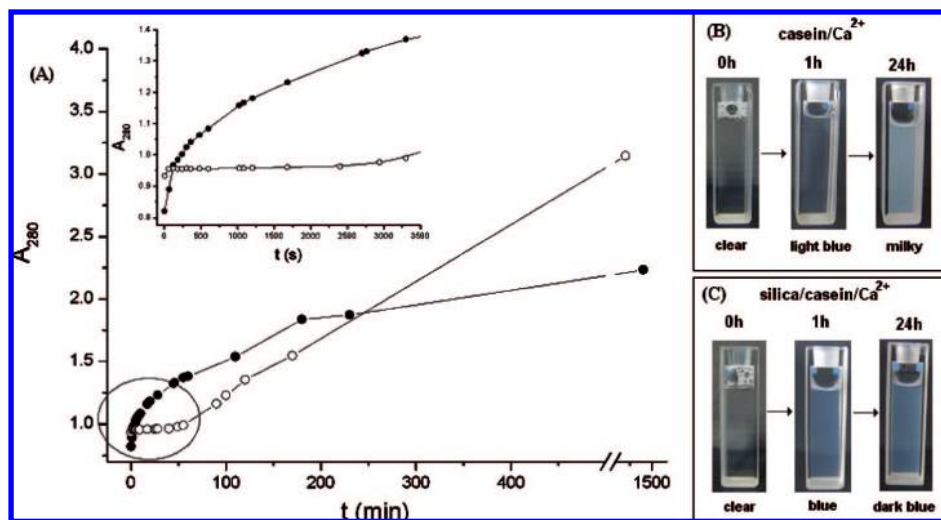
Figure 4. (A) Changes of the absorbance at 280 nm during aging of casein/Ca^{2+} solution (○) and silica/casein/Ca^{2+} solution (●). Inset is the enlarged image of the surrounded area. (B, C) Visual observations made during the absorbance measurements showing the transition from colorless sols to either a milky casein/Ca^{2+} solution (B) or a blue silica/casein/Ca^{2+} solution (C) within 24 hours. The cuvette labeled with "0 h" corresponds to the solution before the addition of calcium, that is, Na caseinate solution (B) and alkaline silica−casein solution (C).

the hydrodynamic radius (Figure 3) of the resulting aggregates increases slowly with time too. The increase in R_H is likely due to the formation of SiO_2 particles. Of particular interest is that the presence of the protein controls the silica particle size, while in the absence of casein, macroscopic flocs (see section 3.1.1.) that settle down very quickly are formed.

3.4.2. Later Stage of the Precipitation Process. Between 1 and 24 h, the bluish solution (Figure 4C) is more intense and the absorbance at 280 nm increases slowly (Figure 4A). In addition, after 24 hours in contact with atmospheric CO_2, hemispherical $CaCO_3$ crystals are precipitated (Figure 5).

Figure 5 shows the experimental data referring to the dependence of the average particle size on the concentration of the casein. It is found that the particle diameter decreased sharply, from 100 to 30 μm, when the concentration of casein was increased to 0.5 g/L, but further increase has almost no effect on this index. When the concentration of the solution is lower than 0.5 g/L, the precipitation process leads to a low number of big particles (Figure 5A,B), whereas at high casein concentration a very high number of small particles (Figure 5C−E) is observed (cf. the ionotropic effect,[34,35] interaction process between organic and inorganic phases). The particle morphology changes from a hemispherical shape to a cracked hemispherical shape upon increase of the concentration of the protein above its critical micelle concentration, cmc $\approx$ 0.5 g/L,[36,37] in aqueous solutions. These hemispherical particles are flat on one side and curved outward on the other side. The flat surface cracks to display a star-like shape (Figure 5D). Occasionally, in the origin of the cracks, "layer-by-layer" sphere-like particles (Figure 5E) grow, probably due to a secondary nucleation. Nevertheless, the casein concentration plays a role in the morphology of hemispherical crystals. As stated before, in the absence of silicate ions, the precipitation of visible calcium carbonate does not occur. Thus, the silicate ions play a role as nucleator for the calcium carbonate mineralization process.

Figure 6 shows the particle diameter, calculated from optical images of the particles versus the reaction time in a 1 g/L casein solution. It is observed from the plot that during the first 9 h, no visible precipitates are detected in the reaction cell. After 10 h, a small amount of crystals with an average size of 3−5 μm is observed. The crystal size sharply increases with the aging
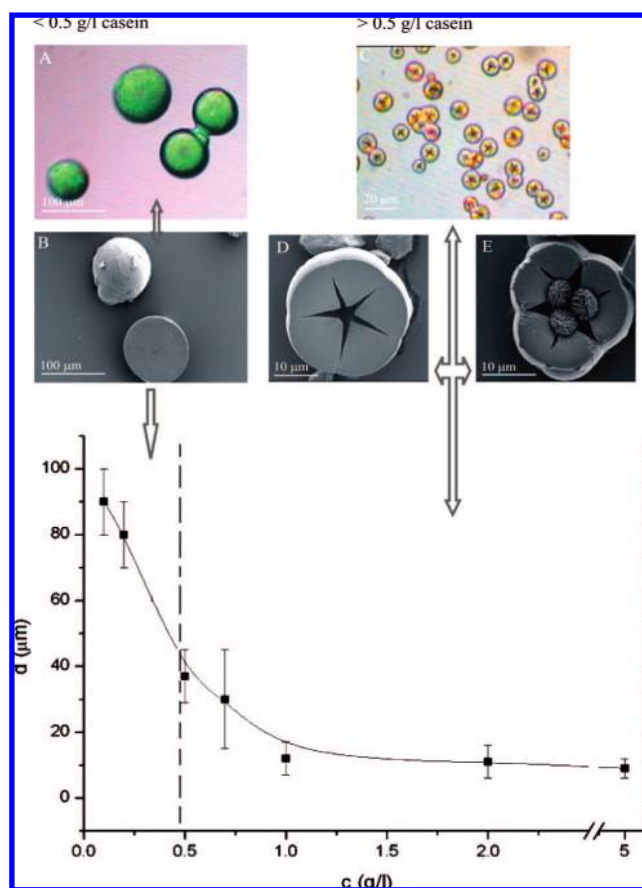

Figure 5. The dependence of the average size of SiO_2/casein/$CaCO_3$ three-composite particles as a function of increasing casein concentration: (A−E) Optical micrographs and SEM images of the hemispherical crystals. [TEOS] = 7.5 mM; [Ca^{2+}] = 7 mM; pH = 11; t = 24 h.

time. After an aging period of 24 h, the particle reached an average size of about 15 μm.

3.4.3. Morphogenesis of Particles. To get more information about the self-organization process of the observed particles, we tried to monitor the morphological evolution of the big polycrystalline particles (Figure 7). After 10 h, the particles around 5 μm have a hemispherical shape being convex on one
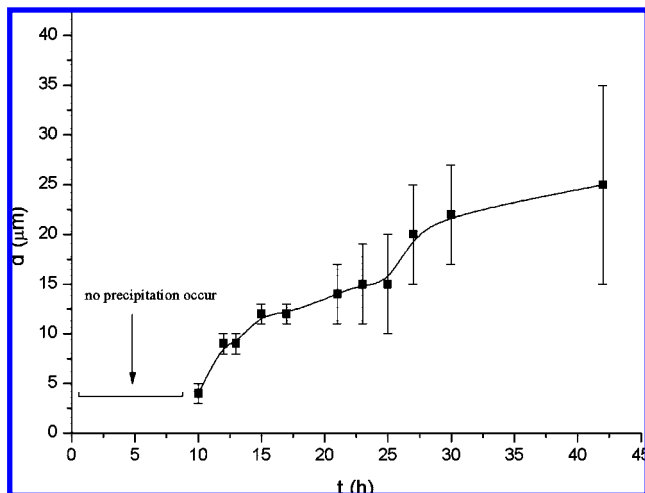
Initiation of Vaterite−Aragonite CaCO₃ Particles

J. Phys. Chem. C, Vol. 112, No. 45, 2008 **17503**

Figure 6. Dependence of the particle size on the reaction time of SiO_2/casein/$CaCO_3$. [TEOS] = 7.5 mM; [casein] = 1 g/L; [Ca^{2+}] = 7 mM; pH = 11; T = 20 °C.

side and concave on the other surface (Figure 7A). The convex outer surface is fully continuous, while in the center of the concave inner surface, the particle starts to crack. Due to the breakage, we can see that the particles are not hollow (Figure 7A, inset). With time, the concave inner surface develops into a flat surface, where the cracks display always a star-like shape (Figure 7B). We note that the plano-convex shape is not an issue of the cell walls because the particles lay on the cell bottom with the crack side up (Figure 5C).

The formation of cracks on the concave side of the particles indicates stress release and a different composition from the convex side (Figure 7B). One explanation could be the initial formation of ACC, which later crystallizes under significant volume decrease (density of ACC is about 1.6 g/mL;[38] that of crystalline $CaCO_3$ is around 2.7 g/mL[39]). This can very well create stresses large enough to crack the overall particle, even if the formed crystals inside the superstructure are $CaCO_3$ nanocrystals.

Occasionally, on the flat surface, partially crystalline silica particles (i.e., the coproduct of the reaction formed in the solution at the early stage) of around 20 nm stick and accumulate (Figure S₆, Supporting Information). Subsequently, the silica spheres are assembled in an edge-to-edge growth[40] (Figure 7C,E) with the gradual enlargement of 2D nanosheet surface areas that are very thin, with a thickness less than 300 nm. In time, the nanosheets develop into layer-by-layer[41] sphere-like particles (Figure 7D) consisting of numerous interconnected nanosheets (Figure 7F). Probably, the casein plays an important role in the formation of integrated nanosheets and multilayered structures.

Simultaneously, the particle grows and the cracks enlarge more and more until it cleaves into small crystal fragments (Figure 8).

3.4.4. Chemical Composition. The EDX spectra, obtained from area indicated in Figure 8C by C_1 and C_2, are consistent with the bulk composition provided by the synthesis. By comparing the two spectra (Figure S₇, Supporting Information), one can notice that the spectrum of the region labeled with C_1 shows a nitrogen peak (see arrow), which comes from the protein and is not found in the region labeled C_2. Both peaks of Si and Ca are smaller in the C_1 area than in the area denoted by C_2. From these observations, it follows that these particles are composites consisting of silica/casein/$CaCO_3$ with two notable differences. First, the casein concentration is consider-

ably lower in the layer-by-layer sphere-like particles than in the rest of the composite, and second, the concentration of silicate and calcium ions is significantly higher in the layer-by-layer sphere-like particles.

3.4.5. Crystal Polymorphism. Figure 9 shows the infrared absorption spectrum of the composites. A comparison of the bands at 746, 877, 1088, 1442, and 1480 cm⁻¹ with standard IR spectra of vaterite-type calcium carbonate reported by Anderson et al.[42] suggests that the structure contains the vaterite calcium carbonate crystal phase. Along with the vaterite bands, the spectrum reveals bands at 1660 cm⁻¹ and in the range of 2000−3500 cm⁻¹, attributed to the OH^- and water vibration. Since the vaterite crystal phase is anhydrous, we believe that the hydration bands are due to the presence of casein and silica in the composite in good agreement with the EDX data. However, the water bands can indicate also the presence of amorphous calcium carbonate ($CaCO_3 \cdot H_2O$) in the composite, thus explaining the formation of the crack on the concave side of the particles. Nevertheless, it should be mentioned that the typical ACC peaks of 866, 1420, and 1476 cm⁻¹ were not observed.

The presence of vaterite phase in the composites is reinforced by powder XRD data. The XRD pattern (Figure 10) exhibits only reflection peaks characteristic of the vaterite phase (V_{110}, V_{112}, V_{114}, V_{300}, V_{304}, V_{118}, and V_{224}). However, the selected area electron diffraction pattern (Figure 7F, inset) recorded on crushed layer-by-layer sphere-like particles indicates the presence of aragonite as the crystalline phase. The lack of aragonite peaks in the XRD is certainly owing to its low mass percentage, which is below the detection limit of the X-ray and FTIR diffractometer.

4. Discussion

Some anomalies that appear in the body, such as calculus, ganglions, or gallstones, are due to organic−inorganic biological systems. Organic and inorganic molecules serve as nucleators, modifiers, or matrices and induce the biomineralization process, which results in unique inorganic−organic composites. Inspired by the biomineralization process, one can try to use organic−inorganic systems in an effort to synthesize $CaCO_3$ materials in vitro with a comparable range of properties. At the moment, extensive reports[43,44] on biomimetic mineralization of calcium carbonate with a large number of additives have been written. Additionally, there are already many reviews that specifically address the synthesis of inorganic crystals or hybrid inorganic/organic materials with specific size, shape, orientation, complex form, and hierarchy.[45−47] The present study shows that silicate ions change the protein structure, while in turn inducing the vaterite calcium carbonate mineralization.

4.1. The Addition of Ca^{2+} ions to the Alkaline Silica Solution and, Subsequently, the Diffusion of Atmospheric CO_2. The addition of $CaCl_2$ and subsequent diffusion of atmospheric CO_2 to the alkaline silica solution result in the formation of deformed crystals (calcite and aragonite) and silica macroscopic flocs as a coproduct of the reaction. The silica particles form owing to the presence of calcium ions, which decrease the solubility of amorphous silica in water, the commonly termed "salting out" effect. Marshall et al.[28] show that as the hydration number of the added cations increases, the solubility of amorphous silica particles decreases. The calcium cations having a very high hydration number (i.e., H = 12) bind the "free" water molecules and decrease the solubility of silica. Qualitatively, a lowered amount of "free" water would be expected to lower silica solubility, and this is
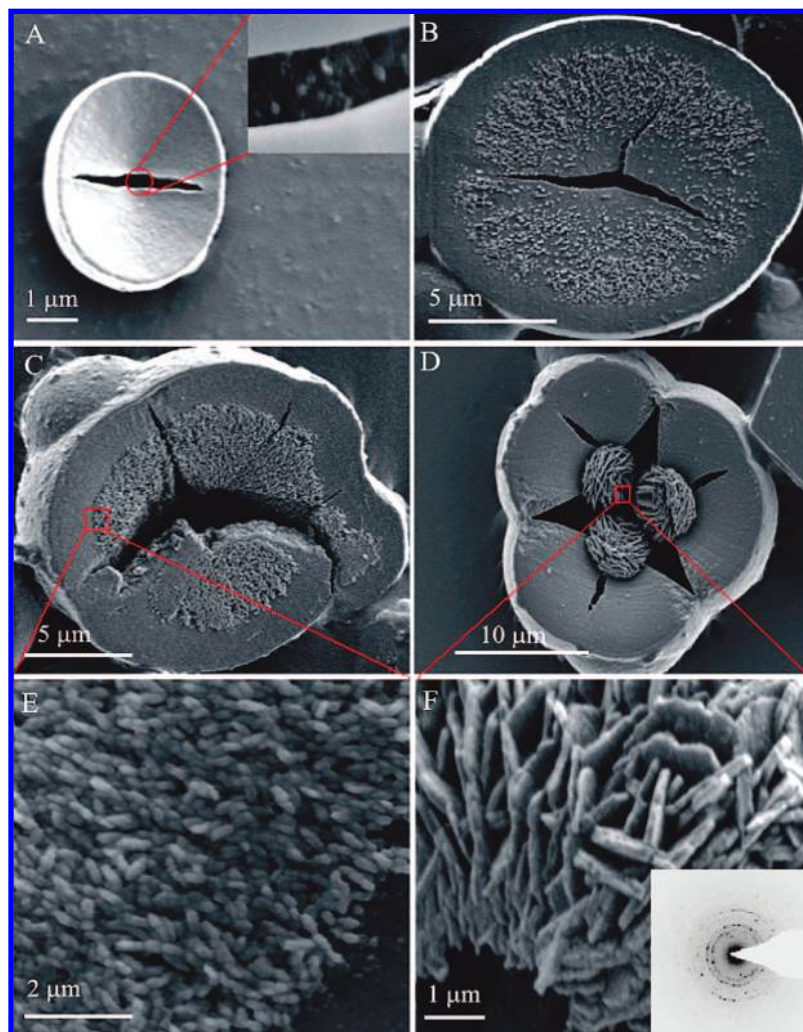
Figure 7. FE-SEM images of self-assembled SiO_2/casein/$CaCO_3$ aggregates, which show the morphological evolution of the composite: (A) early hemispherical particle with a concavo-convex form that cracks on the concave side (inset, the material from the particle interior); (B) hemispherical particle showing how the flat surface cracked to display a star-like shape and, around the crack, silica particles accumulate; (C, D) hemispherical particles showing how the silica particles penetrate into the surface and the layer-by-layer sphere-like particles inside the crack, respectively; (E) enlarged image of the silica sphere arrangement; (F) enlarged image of the multilayered structure and electron diffraction pattern. [TEOS] = 7.5 mM; [casein] = 1 g/L; [Ca^{2+}] = 7 mM; [EtOH] = 0.17%; pH = 11; T = 20 °C.
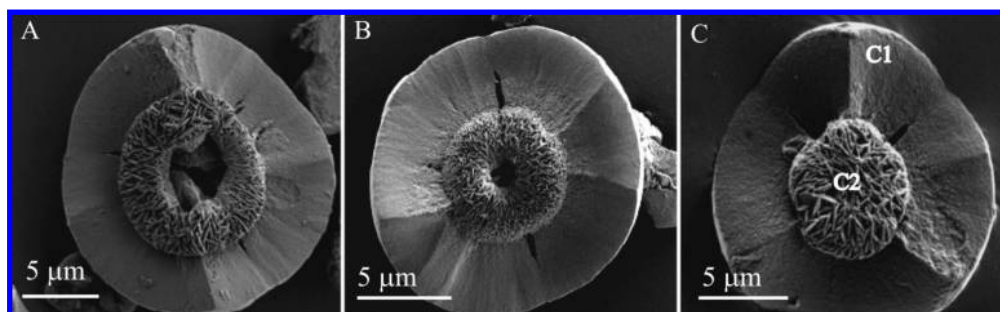

Figure 8. Crystal fragments from the originally cracked hemispherical particle showing the formation of the layer-by-layer sphere-like particles.

what is actually observed. We checked this effect by analyzing three other alkali metal cations, that is, Mg^{2+} (H = 13), Sr^{2+} (H = 2), and Ba^{2+} (H = 1). As expected, the addition of magnesium ions to hydrolyzed TEOS solutions induce also cloudiness in the mixture immediately, and the turbidity is more enhanced than with silica–calcium solution, whereas comparable silica–strontium and silica–barium solutions are isotropic. Furthermore, it must be also considered that Ca^{2+} is a bivalent cation, which can simply cross-link the negative silicate species and induce the coagulation process.

4.2. The Addition of Ca^{2+} Ions to Na Caseinate Sol and, Subsequently, the Diffusion of Atmospheric CO_2. DLS studies on sodium caseinate sols in the absence of calcium show a bimodal distribution consisting of small (as the dominant species, ∼90%) and big aggregates with radii of 18 and 200 nm, respectively. According to the literature, the radius of 20 nm corresponds to casein submicelles[17−19] and the radius of 200 nm corresponds to casein micelles.[15,16] The casein submicelles are composed of 20−25 casein molecules kept together mainly by hydrophobic interactions between proteins.[48]
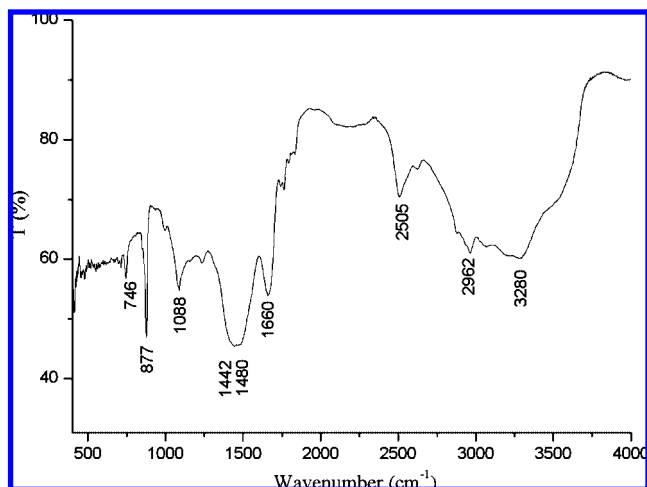
Initiation of Vaterite–Aragonite CaCO₃ Particles

J. Phys. Chem. C, Vol. 112, No. 45, 2008 **17505**

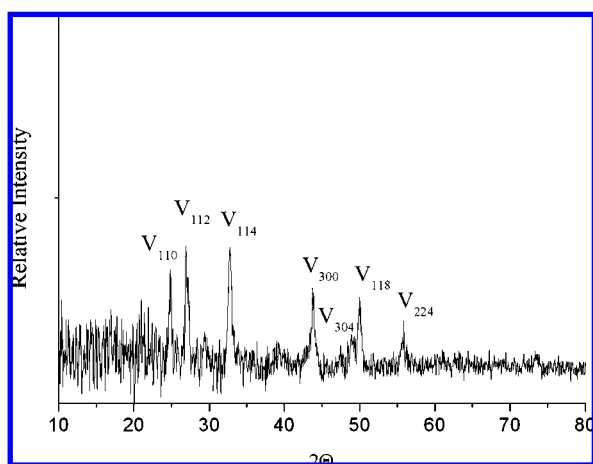**Figure 9.** FTIR spectrum of the SiO₂/casein/CaCO₃ composite particle.

Figure 10. XRD pattern of the SiO₂/casein/CaCO₃ composite particles.

The serine monophosphate NMR signal provides information about the casein conformation in solution. Kakalis et al.[49] showed that the overlapping serine monophosphate peak of the casein micelle spectrum could be resolved into four asymmetric peaks in the casein submicelle spectrum. The casein spectrum presented in Figure 2 is comparable to that reported by Kakalis et al.[49] for casein submicelles.

The addition of calcium to the sodium caseinate solution and, subsequently, the diffusion of atmospheric CO_2 induce no change in the hydrodynamic radius and in the absorbance A_{280} within 1 h, whereas between 1 and 24 h, the absorbance increases and the solution become milky. According to the literature,[50–52] the increase in the turbidity is attributed to the formation of casein micelles from the hydrophobically associated casein submicelles through calcium–side-chain salt bridges. These calcium–protein interactions were caused by binding the calcium ions to both phosphate and carboxylate groups of glutamate and aspartate residues. On one hand, the calcium–phosphate interaction was demonstrated using ³¹P NMR analysis.[49] On the other hand, the calcium–carboxylate interactions were proven by examination of FTIR difference spectra of casein with and without calcium, which reveal changes in the position of carboxylate bands when the calcium ions are present in the solution.[53] Another proof that calcium is implicated in such interactions is the current study, which showed that when the solution was in contact with the atmospheric CO_2, no visible

calcium carbonate particle are precipitated after 24 hours or even after 4 days. This demonstrates that almost none of the added calcium remains in the soluble phase to bind with CO_3^{2-}. Moreover, after four days, the solution has a gelled appearance due to the increased osmotic compressibility of the colloidal system.[54] Dalgleish suggested that the increase in the coagulation rate of the casein sols arises from the neutralization of negative charges within the micelles, causing a decrease in repulsion allowing the close approach, thereby promoting hydrophobic interactions, which are necessary for gel formation to occur.[55]

4.3. The Addition of Ca²⁺ Ions to the Silica–Na Caseinate Solution and, Subsequently, the Diffusion of Atmospheric CO₂. Examination of ³¹P NMR difference spectra of casein sols with and without silicate ions revealed direct evidence for the interaction between silicate ions and serine phosphate groups. Silica and phosphoserin groups, as well as aspartate and glutamate residues of the protein, are negatively charged. The amine-containing residues should be almost neutral at the pH of 11 close to the pK_a of most of these basic amino acids. So, an electrostatic interaction can almost be excluded. Previously, the identification of a Si–serine interaction was provided by ²⁹Si, ¹³C, and ¹⁷O NMR shifts. These complexes involve H-bonds or direct C–O–Si covalent bonds.[5–11] Additionally, we performed an NMR experiment in the presence of urea (6 M), a hydrogen bond disrupter, in order to probe the hydrogen bond formation between silicate ions and the protein. We observed no change in the NMR signals of the silicate–casein solution and silicate–casein–urea solution. So, hydrogen bond formation is also excluded. A transesterification of phosphate against silicate in the phosphoserin residues leading to a covalent C–O–Si bond also seems unlikely because the NMR signal for serine monophosphate group did not disappear, it is only shifted upfield. For the moment, we are not able to explain the type of the interaction between silica and the protein. However, we suppose that the silica species should interact with the serine monophosphate groups (assumption based on the NMR measurements) and, in turn, block these groups against precipitation with calcium.

The addition of calcium to the silicate–caseinate solution and, subsequently, the diffusion of atmospheric CO_2 induce an increase in the hydrodynamic radius and in the absorbance A_{280} intensity. We assign this increase to the formation of silica particle with added calcium due to the 'salting-out' effect. A comparable effect is observed when calcium is added to an alkaline silica solution, but with a significant difference. The silica particles formed in the alkaline silica sols are about 200 nm, while the particles precipitated in the silica–casein solution are ca. 20 nm in diameter. So, the silica particle size is controlled by the Si–serine complexes. Likewise, the bovine serum albumin–silicate interactions induce protein aggregation that controls silica particle size.[56]

We re-emphasize that particles from silica/casein/Ca²⁺ solution initially increase in size much more compared with those from casein/Ca²⁺, but after ~220 min, the effect is opposite. In the absence of silicate ions, casein being a calcium sponge protein with integrated nucleation sites will bind calcium ions through both phosphate and carboxylate groups of glutamate and aspartate residues and afterwards lead to the formation of casein micelle. In the presence of silicate ions, the calcium nucleation sites on the casein structure are probably blocked and, therefore, calcium will interact with free silica ions from the bulk solution and form silica particles. Further, a strong interaction of calcium with silica in the solution may also occur.

After ∼220 min, the size of silica particles remains almost constant over time because less Ca^{2+} ions are available, whereas the casein/Ca^{2+} solution increases in size much more due to hydrophobic interactions or calcium phosphate linkages.

After 24 hours in contact with atmospheric carbon dioxide, hemispherical calcium carbonate crystals in form of vaterite phase are precipitated, whereas comparable experiments made in the absence of silicate ions do not promote the formation of calcium carbonate particles. This observation suggests that the calcium binding sites of pure sodium caseinate sols, that is, serine-phosphate groups, are likely blocked by silicate ions. Thus, with the addition of calcium ions, the formation of colloidal calcium phosphate is inhibited by silicate ions. According to the literature,[10−16] the calcium ions bind directly with Si−serine complexes, and then the vaterite crystal formation is promoted in agreement with Terashita et al.[57] Occasionally, we saw that in the origin of the cracks, layer-by-layer sphere-like aragonite particles grow probably due to a secondary nucleation.

The formation of layer-by-layer sphere-like particles suggests that the growth process may involve the following steps: (1) At the early stage, tiny silica nanospheres form in the silica−casein supersaturated solution. (2) In time, these nanoparticles stick together and, afterwards, attach to the hemispherical particle surface probably owing to electrostatic interaction between Si−O$^-$ and −NH$_3^+$ groups[58] or Ca^{2+}. (3) The initially formed spheres assemble in an edge-to-edge way with the gradual enlargement of the 2D surface areas. (4) As soon as the 2D nanosheets have been formed, the protein starts selectively absorbing onto the sheets, which leads to the formed nanosheets being glued together. (5) Finally, the arrangement of the 2D sheets into 3D hierarchical microspheres takes place. For the formation of 3D microspheres, a layer-by-layer growth style can be considered.[44]

5. Conclusions

Novel hemispherical three-component vaterite microstructures were obtained in alkaline silica−casein sols by the diffusion of atmospheric carbon dioxide into the solution. The initiation of this process is due to the presence of silicate ions that interact with serine-monophosphate groups and modify the casein structure in aqueous solution and, as a consequence, promote vaterite formation. We conclude that crystallization processes that appear *in vivo* could be influenced by different modifications in protein structures that are controlled by inorganic ions, such as the pulmonary calcification process.

Supporting Information Available: SEM image of the precipitate obtained and XRD pattern of silica particles after mixing the $CaCl_2$ with alkaline silica solutions, FT-IR spectra of the pure SiO_2 and of the precipitate that formed upon mixing calcium chloride and alkaline TEOS sols, optical micrographs of the $CaCO_3$ crystals, XRD pattern of the $CaCO_3$ crystals, and TEM image of amorphous silica particles. This material is available free of charge via the Internet at http://pubs.acs.org.

References and Notes

(1) Wiercinski, F. J. *Biol. Bull.* **1989**, *176*, 195.
(2) Damen, J. J. M.; Ten Cate, J. M. *J. Dent. Res.* **1989**, *68* (9), 1355.
(3) Campbell, A. K. *Surv. Biochem. Anal.* **1988**, *19*, 485.
(4) Cutress, T.W. *Arch. Oral Biol.* **1972**, *17*, 1081.
(5) Hecky, R.; Mopper, K.; Kilham, P.; Degens, T. *Marine Biol.* **1973**, *19*, 323.
(6) Sullivan, C. W. *Silicification by Diatoms in Silicon Biochemistry*; Ciba Foundation Symposium 121, John Wiley: Chichester, U.K., 1986.
(7) Pickett-Heaps, J; Schmidt, A. M.; Edgar, L. A. *Prog. Phycol. Res.* **1990**, *7*, 1.
(8) Frauso da Silva, J. J. R.; Williams, R. J. P. *The Biological Chemistry of the Elements: The Inorganic Chemistry of Life*; Clarendon Press: Oxford, U.K., 1991.
(9) Swift, D.; Wheeler, A. P. *J. Phycology* **1992**, *28*, 202.
(10) Lobel, K. D.; West, J. K.; Hench, L. L. *Marine Biol.* **1996**, *126*, 353.
(11) Kinrade, S. D.; Del Nin, J. W.; Schach, A. S. *Science* **1999**, *285*, 1542.
(12) LeBlank, J. G.; Matar, C.; Valdéz, J. C.; LeBlank, J.; Perdigon, G. *J. Dairy Sci.* **2002**, *85*, 2733.
(13) Jenness, R. *Milk Proteins, Chemistry and Molecular Biology I*; Academic Press: New York, 1970.
(14) Farrell, H. M., Jr.; Kumosinsky, T. F.; Malin, E. L.; Brown, E. M. *Methods Mol. Biol.* **2002**, *172* (1), 97.
(15) Brunner, J. R. Milk Proteins. In *Food Proteins*; AVI Publishing Company, Inc.: Westport, CT, 1977.
(16) Holt, C.; Horne, D. S. *Neth. Milk Diary* **1996**, *50*, 85.
(17) McMahon, D. J.; McManus, W. R. *J. Dairy Sci.* **1998**, *81*, 2985.
(18) Walstra, P. *Int. Dairy J.* **1999**, *9*, 189.
(19) Rollema, H. S. *Adv. Dairy Chem.* **1992**, *1*, 111.
(20) Wong, N. P. *Fundamentals of Dairy Chemistry*, 3rd ed.; Van Nostrand Reinhold: New York, 1988.
(21) Zhou, Y.; Shimizu, K.; Cha, J. N.; Stucky, G. D.; Morse, D. E. *Angew. Chem., Int. Ed.* **1999**, *38*, 780.
(22) Kröger, N.; Lorenz, S.; Brunner, E; Sumper, M. *Science* **2002**, *298*, 584.
(23) Jiang, L.; Dan, Y. *Colloid Polym. Sci.* **2004**, *282*, 1364.
(24) Jiang, L.; Pan, K.; Dan, Y. *Colloid Polym. Sci.* **2006**, *285*, 65.
(25) Bacs, C. F., Jr.; Mesmer, R. E. *The Hydrolysis of Cations*; Wiley: New York, 1974.
(26) Voinescu, A. E.; Kellermeier, M.; Carnerup, A. M.; Larsson, A.; Touraud, D; Kunz, W.; Hyde, S. T. *J. Cryst. Growth* **2007**, *306*, 152.
(27) Kerr, G. T. *J. Phys. Chem.* **1966**, *70*, 1047.
(28) Marshall, W. L.; Warakoski, M. *Geochim. Cosmochim. Acta* **1980**, *44*, 915.
(29) Imai, H.; Terada, T.; Yamabi, S. *Chem. Commun.* **2003**, *4*, 484.
(30) Matheis, G.; Penner, M. H.; Feeney, R.E.; Whitaker, J. R. *J. Agric. Food Chem.* **1983**, *31*, 379.
(31) Matheis, G.; Whitaker, J. R. *Int. J. Biochem.* **1984**, *16* (8), 867.
(32) Van Hekken, D. L.; Dudley, R. L. *J. Dairy Sci.* **1997**, *80* (11), 2751.
(33) Belton, P. S.; Lyster, R. L. J.; Richards, C. P. *J. Dairy Res.* **1985**, *52* (1), 47.
(34) Addadi, L; Moradian, J.; Shay, E.; Maroudas, N. G.; Weiner, S. *Proc. Natl. Acad. Sci. U.S.A.* **1987**, *84*, 2732.
(35) Voinescu, A. E.; Touraud, D.; Lecker, A.; Pfitzner, A.; Kunz, W.; Ninham, B. W. *Langmuir* **2007**, *23* (24), 12269.
(36) Schmidt, D.G.; Payens, T. A. *J. Colloid Interface Sci.* **1972**, *39*, 655.
(37) Leclerc, E.; Calmettes, P. *Phys. Rev. Lett.* **1997**, *78*, 150.
(38) Bolze, J.; Peng, B.; Dingenouts, N.; Panine, P.; Narayanan, T.; Ballauff, M. *Langmuir* **2002**, *18*, 8364.
(39) Pennington, T. J.; Strathmann, R. R. *Biol. Bull.* **1990**, *179*, 121.
(40) Li, Y.; Liu, J.; Huang, X.; Li, G. *Cryst. Growth Des.* **2007**, *7* (7), 1350.
(41) Zhou, G.; Lü, M.; Yang, Z.; Tian, F.; Zhou, Y.; Zhang, A. *Cryst. Growth Des.* **2007**, *7* (2), 187.
(42) Anderson, F. A.; Brecevic, L. *Acta Chem. Scand.* **1991**, *45*, 1018.
(43) Meldrum, F. C.; Hyde, S. T. *J. Cryst. Growth* **2001**, *231*, 544.
(44) Deng, S. G.; Cao, J. M.; Feng, J.; Guo, J.; Fank, B. Q.; Zheng, M. B.; Tao, J. *J. Phys. Chem. B* **2005**, *109*, 11473.
(45) Dabbs, D. M.; Aksay, I. A. *Annu. Rev. Phys. Chem.* **2000**, *51*, 601.
(46) Cölfen, H. *Curr. Opin. Colloid Interface Sci.* **2003**, *8*, 23.
(47) Cölfen, H. *Top. Curr. Chem.* **2007**, *271*, 1.
(48) Kumosinsky, T. F., Jr *Protein Chem.* **1991**, *10* (1), 3.
(49) Kakalis, L. T.; Kumosinski, T. F.; Farell, H. M. *Biophys. Chem.* **1990**, *38*, 87.
(50) Chu, B.; Zhou, Z.; Wu, G., Jr *J. Colloid Interface Sci.* **1995**, *170*, 102.
(51) Farrell, H. M., Jr.; Thompson, M. P. *Caseins as Calcium Binding Proteins*; CRC Press, Inc.: Boca Raton, FL, 1988; Vol 2.
(52) Famelart, M. H.; Le Graet, Y.; Raulot, K. *Int. Dairy J.* **1999**, *9*, 293.
(53) Byler, D. M., Jr *J. Dairy Sci.* **1989**, *72* (7), 1719.
(54) De Kruif, C. G. *J. Dairy. Sci.* **1998**, *81*, 3019.
(55) Dalgleish, D. G. *Adv. Dairy Chem.* **1992**, *1*, 779.
(56) Coradin, T.; Coupé, A.; Livage, J. *Colloids Surf. B* **2003**, *29*, 189.
(57) Terashita, M.; Ikegami, T. *Jpn. Kokai Tokkyo Koho* **1989**, JP 01192719 A 19890802, written in Japanese.
(58) Coradin, T.; Livage, J. *Colloids Surf. B* **2001**, *21*, 329.